Published in final edited form as:
Nat Neurosci. ; 14(8): 1045–1052. doi:10.1038/nn.2876.

Differential tuning and population dynamics of excitatory and inhibitory neurons reflect differences in local intracortical connectivity

Sonja B. Hofer[#1], **Ho Ko**[#1], **Bruno Pichler**[1,5], **Joshua Vogelstein**[3], **Hana Ros**[1], **Hongkui Zeng**[4], **Ed Lein**[4], **Nicholas A. Lesica**[2], and **Thomas D. Mrsic-Flogel**[1]

[1]Department of Neuroscience, Physiology and Pharmacology

[2]Ear Institute, University College London, London, UK

[3]Johns Hopkins University, Baltimore, USA

[4]Allen Institute for Brain Science, Seattle, USA

[#] These authors contributed equally to this work.

Abstract

Neuronal responses during sensory processing are influenced both by the organization of intracortical connections and the statistical features of sensory stimuli. How these intrinsic and extrinsic factors govern activity of excitatory and inhibitory populations is unclear. Using two-photon calcium imaging *in vivo* and intracellular recordings *in vitro*, we investigated the dependencies between synaptic connectivity, feature selectivity and network activity in pyramidal cells (PCs) and parvalbumin-expressing fast-spiking (PV/FS) interneurons in mouse visual cortex. In PC populations, patterns of neuronal correlations were largely stimulus-dependent, indicating that their responses were not strongly dominated by functionally biased recurrent connectivity. In contrast, visual stimulation only weakly modified co-activation patterns of PV/FS cells, consistent with the observation that these broadly tuned interneurons received very dense and strong synaptic input from nearby PCs with diverse feature selectivities. Therefore feedforward and recurrent network influences determine the activity of excitatory and inhibitory ensembles in fundamentally different ways.

Introduction

The capacity of the neocortex to process sensory information depends on neuronal interactions between excitatory and inhibitory cell types. However, the relationships between

Correspondence should be addressed to T.D.M.F. (t.mrsic-flogel@ucl.ac.uk).
[5]Present address: National Institute for Medical Research, Mill Hill, London, UK

Author contributions

S.B.H. and H.K. performed all in vivo and slice experiments. S.B.H., H.K., N.L. and T.D.M.-F. analyzed the data. H.R. carried out antibody labeling. B.P. developed image acquisition software and the program for extracting calcium transients. J.V. developed spike inference algorithms. E.L. and H.Z. generated and supplied the mice. S.B.H., H.K., N.L. and T.D.M.-F. wrote the paper.

Europe PMC Funders Author Manuscripts

connectivity, receptive field properties and network dynamics of different cell types are not fully understood.

The large majority of cortical neurons are sparsely interconnected excitatory pyramidal cells (PCs) that typically exhibit selective responses to different sensory features, and provide the main route of information flow to and from cortical areas. The remaining ˜20% of cortical neurons consist of different subclasses of GABAergic inhibitory interneurons, which influence the firing and sensory responses of nearby PCs1–6.

In contrast to PCs, parvalbumin-expressing (PV) fast-spiking (FS) interneurons, which form the largest inhibitory subgroup1,2, form denser connections within local circuits7–9. The fraction of local excitatory inputs sampled by FS cells remains unclear, since reports vary from 19 %10 up to 60 %7 even in primary visual cortex (V1) of the same species (rat). The differences in connectivity between PCs and FS interneurons may influence the specificity by which these neuronal subpopulations respond to sensory stimuli, and the extent to which their co-activations are determined by sensory drive.

In V1, most layer 2/3 PCs respond selectively to oriented grating stimuli, possibly reflecting their non-random connectivity, whereby feedforward inputs from layer 4 and recurrent inputs from layer 2/3 are provided preferentially by neurons with similar response preferences11–15. On the other hand, there is considerable debate about the selectivity of visual responses and the functional organization of connectivity of PV/FS interneurons. In V1 of higher mammals, where neurons are arranged in functional columns, FS interneurons are often selective for orientation16–18. In mouse V1, where neurons with different orientation preferences are locally intermixed, PV/FS cells and inhibitory neurons in general are reported to be more broadly tuned19–21 (but see ref. 22). These findings suggest that FS interneurons receive non-selective excitatory input from the surrounding network23, and hence are more sharply tuned in species with orientation maps, but less well tuned in mice where neighboring PCs exhibit diverse visual feature selectivity20. However, others find sharp orientation tuning of many PV/FS interneurons in mouse V122, suggesting that they receive input from sub-networks of PCs with similar orientation preference10. Discerning between these apparently conflicting results is crucial for understanding the specificity by which these inhibitory neurons respond to sensory stimuli and influence responses of other neurons in the network. It is therefore important to determine the response selectivity of a defined population of inhibitory neurons and, at the same time, any functional biases of their connectivity in the local circuit.

With differences in their local connectivity, populations of PCs and PV/FS interneurons may also be expected to differ in their network interactions and in the way their activity patterns are influenced by sensory stimuli. The organization of intracortical connections is thought to be reflected in patterns of spontaneous activity24. Some studies report similar patterns of spontaneous and evoked activity24–29, suggesting that intracortical connections influence activity patterns, such that a neuron is likely to fire with the same interacting partners (ensemble) in the presence and absence of sensory input. In contrast, other studies show that even functionally similar neurons can fire independently of each other and that the strength of correlated firing in pairs of neurons can be influenced by sensory input30–35. At the level

of local circuits, therefore, the degree to which sensory-evoked co-activations are influenced by intrinsic biases in connectivity, and how this relates to cell type, remain unresolved.

In this study we investigated the relationship between local synaptic connectivity, sensory response properties and the structure of network correlations in populations of PCs and PV/FS interneurons in the same neuronal circuit. We applied two-photon calcium imaging36 in layer 2/3 of mouse V1 to record spontaneous and visually evoked population activity with single-cell resolution37,38, as well as to identify PV neurons genetically labeled with a red fluorescent protein39. We then used patch-clamp recordings in slices of the same tissue to determine local connectivity between a subset of neurons whose visual response properties were characterized *in vivo*. We found fundamental differences in both local synaptic connectivity and stimulus-dependence of neuronal co-activations in populations of PCs and PV/FS interneurons, indicating that the balance between feedforward and recurrent input differ across cortical cell types during processing of visual information.

Results

Visual responses of PV interneurons

We first measured the orientation tuning of genetically targeted red fluorescent PV cells, using PV-Cre mice crossed to a Cre-responsive reporter line (Ai9-lsl-tdTomato)39. Immunocytochemistry confirmed that red cells in layer 2/3 were almost exclusively PV-containing (92 %, Supplementary Fig. 1). Electrophysiological properties of most red cells were typical of fast-spiking (FS) interneurons and none showed characteristics of excitatory pyramidal cells (Supplementary Fig. 1). We simultaneously imaged calcium signals and recorded action potential (AP) firing in PV cells by carrying out *in vivo* two-photon targeted loose-patch recordings of red cells in monocular V1 that was bulk labeled with injections of the calcium indicator dye OGB-1-AM (Fig. 1a-e). Confirming previous results20, changes in AP firing were reflected in the calcium signal, even for neurons with high firing rates (Fig. 1b-e, Supplementary Figs. 2, 3 and 4). For both putative PCs and fast-spiking PV cells the preferred orientation and the orientation selectivity (OSI) calculated from calcium signals were highly similar to values obtained from spiking responses (Fig. 1f,g). Calcium transient amplitude correlated well with the number of recorded APs for all cells (Fig. 1d, Supplementary Fig. 2e). Interestingly, the slope of this correlation varied between cells, partly depending on the maximum firing rate. When the size of the calcium transients was plotted against AP number normalized to the maximum firing rate (for the range of gratings presented), a relatively similar (and nearly linear) relationship was apparent for all PV cells (Fig. 1e). A clear correspondence was also observed between recorded APs and firing rate inferred from the calcium signal using a fast non-negative deconvolution method40 (see Methods) for both putative PCs (Supplementary Fig. 2) and PV neurons (Supplementary Fig. 4).

Having thus established that the calcium signal is a good indicator for changes in AP firing for neurons with very different firing frequencies, we used two-photon imaging to measure orientation selectivity for significantly responsive (see Methods) populations of PV neurons and neurons not expressing the red protein (Fig. 1h-j), which primarily (≥ 90 %) represent excitatory PCs2, and will therefore be referred to as PCs in the remainder of the manuscript.

As expected, most PCs responded selectively to oriented gratings and, exhibited on average, high orientation selectivity41 (Fig. 1i,j, median OSI = 0.60). As a population, PV neurons responded much less selectively to moving gratings, as the majority showed broader orientation tuning (Fig. 1i,j, median OSI = 0.26), as was also apparent from the cell-attached recordings (Fig. 1g, median $OSI_{spiking}$ = 0.13). However, it should be noted that many PV neurons did exhibit some orientation preference, including a smaller fraction more selective for orientation (Fig. 1i,j; OSI > 0.4 in 13/71 or 18% of significantly responsive PV neurons).

Cell type specific differences in synaptic connectivity

In layer 2/3 of rodent V1, PCs connect to each other sparsely7,11,12,23 whereas FS interneurons, which typically express PV and constitute up to 10% of the cortical neuronal population2, are more densely connected to the surrounding network7–9. PCs may form selectively interconnected subnetworks consisting of neurons with similar visual feature selectivity12, while FS interneurons receive functionally unbiased input from surrounding pyramidal neurons and are hence more broadly tuned20,23. To test these hypotheses directly, we developed an approach to map synaptic connectivity between nearby neurons (<50 μm apart) whose visual response properties had been functionally characterized in vivo11. We identified the same neurons in slices that had been imaged *in vivo*, and therefore were able to directly relate connectivity of different neurons to their orientation tuning (Fig. 2, also see Methods). By patch clamp recordings from up to four neurons simultaneously, connectivity was assessed by stimulating one neuron at a time and observing postsynaptic potentials (PSPs) in each of the other neurons in turn. The presence or absence of short-latency PSPs enabled us to determine the incidence and strength of synaptic connections. With this approach, we tested the dependency of connection probability on orientation tuning of PCs and FS interneurons.

We previously found that layer 2/3 PC-PC connections in mouse V1 were weak and sparse (19%, 45 connections out of 235 tested; Fig. 2d, e), and preferentially but not exclusively formed between neurons with smaller difference in preferred orientations11 (ΔOri, Fig. 2h). In contrast, here we show that PV/FS interneurons received input from neighboring PCs with remarkably high probability (88%, 36 of 41 tested, data from wild-type and PV-Cre-lsl-tdTomato mice, see Methods; Fig. 2d). Figures 2a, f and g show the orientation tuning curves for 17 FS cells together with the tuning profiles of PCs responsive to moving gratings from which they received excitatory connections. PV/FS interneurons exhibited weak biases towards orientation (OSI range: 0.11 – 0.51; median = 0.22), and received inputs from both sharply and more broadly tuned PCs (OSI range: 0.07 – 1.00; median = 0.68) preferring a wide range of orientations/directions (Fig. 2a,f,g). As shown in our previous study, among orientation selective PCs (OSI > 0.4), the connectivity rate decreased monotonically with increasing difference in ΔOri11 (P = 0.04, Cochran-Armitage test for trend, Fig. 2h). In contrast, no trend was observed for PC-PV/FS connection probability (P = 0.53, Cochran-Armitage test), because almost all PCs provided input to neighboring PV/FS interneurons irrespective of how similarly they responded to visual stimulation or how selectively they responded to grating orientation (Fig. 2h). Moreover, the strength of most PC-PV/FS connections was an order of magnitude higher than PC-PC connections (median EPSP amplitude of PC-FS = 1.36 mV vs 0.20 mV for PC-PC connections; $P < 10^{-8}$, rank sum test,

Fig. 2e), a finding consistent with previous results in rat V17. We additionally tested if the strength of connections from PCs to PV/FS cells or their short-term plasticity (paired-pulse-ratio, PPR) depended on the similarity of orientation tuning between two neurons (Figs. 2i,j), but did not find significant trends ($P > 0.1$).

These results indicate that FS neurons receive very dense and strong input from nearby pyramidal neurons with diverse selectivities and preferences for stimulus orientation, and this connectivity likely contributes to the broader tuning of FS interneurons.

Relationship between spontaneous and evoked activity

We next investigated the extent to which differential connectivity profiles of PCs and PV/FS cells may influence the activity dynamics of these two neuronal populations. We recorded spontaneous calcium signals in the dark in layer 2/3 of V1 in PV-Cre-lsl-tdTomato mice and computed correlations of time-varying calcium signals for each neuronal pair over the duration of each recording (spontaneous correlation). Pair-wise correlations provided an indication of which neurons were likely to be co-active spontaneously. Given that spontaneous activity patterns have been suggested to reflect underlying connectivity in the network[24,25], we expected the relationship between spontaneous correlations and visual response similarity to resemble the relationship we had observed between visual response similarity and synaptic connectivity[11] (Fig. 2). To test this, we plotted the correlation strength of neuronal pairs during spontaneous activity against signal correlation (correlation of average responses, see Methods), which provides a measure of the similarity of neuronal responses to drifting gratings. We quantified the relationship between spontaneous correlation and signal correlation for pairs of PCs, pairs of PV cells and pairs consisting of one PC and one PV cell, by computing the correlation (R) and the slope of the linear fit (Fig. 3a-c). To visualize data from all animals in a single plot, we additionally normalized the pair-wise correlation values by calculating z-scores separately for each region (Fig. 3d, see Methods), because the average correlation strength varied between regions and animals (see also Fig. 4b) and pooling the raw data together could introduce additional dependencies. Surprisingly, we found only a very weak relationship between spontaneous and signal correlation for PC pairs (Fig. 3a-d, median $R = 0.18$, median slope = 0.04; pooled data: $R = 0.10$; $P < 10^{-4}$); PCs with similar responses to drifting gratings were only slightly more likely to fire together spontaneously than neurons with very different visual responses, and the scatter of data points was very large. A somewhat stronger relationship was apparent for pairs consisting of one PC and one PV cell (Fig. 3a-d, median $R = 0.33$, median slope = 0.14; pooled data: $R = 0.22$, $P < 10^{-4}$). In contrast to PCs, there was a strong relationship between signal and spontaneous correlation for PV cell pairs, whereby cells responding more similarly to gratings were more correlated during spontaneous activity, while those responding less similarly were less correlated during spontaneous activity (Fig. 3a-d, median $R = 0.68$, median slope = 0.49; pooled data: $R = 0.61$, $P < 10^{-4}$).

These results could be influenced by a well documented relationship between correlation strength and cortical distance[30]. We also found a negative relationship between the strength of correlation of the activity of cell pairs with and without visual stimulation and cell distance. This negative relationship was stronger and 2-3 fold steeper for PV cell pairs than

for PC pairs (Supplementary Fig. 5a-c, spontaneous activity: PV, R = -0.32, slope = -0.009; PC, R = -0.12, slope = -0.003). However, restricting our dataset to cell pairs less than 50 μm apart did not alter the relationship between response similarity and spontaneous correlations (Supplementary Fig. 5d-f compare to Fig. 3d), ruling out that they were mostly brought about by distance effects.

Taken together, the weak relationship between spontaneous correlation and visual response similarity in populations of PCs suggests that biased local connectivity among these neurons (Fig. 2) does not appear to have a strong impact on the pattern of network co-activations. In contrast, there was a strong relationship between spontaneous correlation and visual response similarity of PV cells, suggesting that very dense and strong excitatory input from the local network strongly influences their activity during visual stimulation.

Structure of PV cell correlations is less stimulus independent

The results from the previous section suggest that PV cells are influenced more by local network connectivity than PCs. In order to investigate the significance of this difference for visual processing, we tested the similarity between spontaneous activity patterns and those evoked by different types of visual stimuli by presenting both episodically drifting whole-field gratings and sequences of naturalistic movies (Fig. 4a-f, see Methods).

Spontaneous activity was characterized by brief (< 1 s), sporadic events involving multiple neurons, separated by periods in which few neurons were active (Fig. 4a). Presentation of visual stimuli resulted in reproducible patterns of activity and changed network activity in different ways: episodically presented drifting gratings induced epochs of many active neurons (Fig. 4c, corresponding to the periods of grating drift) alternated with periods of almost complete lack of activity in the population (corresponding to periods of no drift). This strong periodic recruitment of the circuit caused the overall strength of time-varying response correlations (total correlations) of calcium signals between PCs to increase compared to those during spontaneous activity (Fig. 4b,d, spontaneous: R = 0.12; gratings: R = 0.20, group medians of imaged regions, P = 0.005, sign rank test). In contrast, continuously presented natural movies significantly de-correlated responses of PCs (Fig. 4e,f, natural: R = 0.09, P = 0.007).

Between PV neurons, time-varying response correlations were on average considerably stronger than between PCs during all conditions (Fig.4b,d,f, spontaneous: R = 0.20; gratings: R = 0.31; natural: R = 0.18; group median of imaged regions, P < 0.0005), and during visual stimulation even stronger than correlations between PV neurons and the surrounding neuropil (Supplementary Fig. 6). Pairs consisting of one PC and one PV cell showed intermediate correlation strength during all conditions (Fig.4b,d,f). Together, these results are consistent with the connectivity profile of PCs and PV cells in the local circuit: PV cells share more common input (Fig. 2), and are more interconnected42,43, and therefore exhibit more correlated activity.

To test whether neurons tended to be similarly co-active or co-inactive during spontaneous activity and during visual stimulation, we determined how the structure of correlations of PC or PV cell populations changed across stimulus conditions. Figure 4g shows matrices of

pair-wise correlations for all cell pairs in one imaged region from recordings of spontaneous activity and during stimulation with episodically drifting gratings or natural movies. If neuronal ensembles which fire together without visual input are also likely to be co-active during visual stimulation, correlation matrices for the different conditions would appear similar. This was the case for populations of PV interneurons, but not for PCs (Fig. 4g). To obtain a quantitative measure of similarity between spontaneous and sensory-evoked co-activation patterns, we calculated the correlation coefficient of the off-diagonal elements between the different matrices, which we term pattern correlation (Fig. 4h). When comparing correlations between PCs across imaged regions, we found that visual stimulation strongly altered correlation patterns present during periods of spontaneous activity (Fig. 4h and Supplementary Fig. 7, group median pattern correlation: spontaneous versus gratings = 0.31, spontaneous versus natural movie = 0.30). Equally large differences in correlation patterns were apparent when comparing population activity driven by different stimuli (Fig. 4h and Supplementary Fig. 7, group median pattern correlation: gratings versus natural movie = 0.29). Therefore, there appears to be only a weak resemblance between patterns of PC co-activations during spontaneous and different stimulus regimes, suggesting that biased local connectivity does not strongly influence how PC populations respond to external input, which allows individual neurons to participate in different ensembles.

In contrast, the degree of correlated activity between pairs of PV cells was largely maintained regardless of whether they were active spontaneously or driven by a visual stimulus (Fig. 4g,h). If two PV cells were strongly correlated during one stimulus condition, they were likely to be strongly correlated in another. Thus, while the patterns of correlated activity among PCs were different between spontaneous and different visually-evoked states, the co-activation patterns in networks of PV cells were very similar (Fig. 4h and Supplementary Fig. 7, group median pattern correlation: spontaneous versus gratings = 0.73, spontaneous versus natural movie = 0.67, gratings versus natural movie = 0.73). Interestingly, pattern correlations for PC/PV cell pairs showed intermediate values (Fig. 4h, group median pattern correlation > 0.47 across all conditions), indicating that the groups of PCs associated with the firing of PV neurons tended to change during different conditions, but not as much as the co-activation patterns in populations of PCs. Calculating pattern correlations across different conditions from inferred spikes instead of the raw calcium signals produced similar results (Supplementary Fig. 8).

Together, these results indicate that the patterns of network co-activations of PCs were more strongly influenced by visual input than co-activations patterns of PV cells, which appeared similar across conditions and suggests that PV cell activities were strongly determined by intrinsic connectivity.

Structure of noise correlations

Although biased recurrent connectivity may not dominate response patterns of PCs, it may still influence them. The differences in total correlations described above do not differentiate whether changes in co-activation patterns are a result of a change in feedforward input due to different stimuli or a change in the state of network activity due to regrouping of local ensembles. To test this, we separated the total correlations between cell pairs into signal and

noise components: signal correlations arise from correlations in the stimulus itself and/or similarity in preferred stimulus features (such as orientation), while noise correlations arise from mutual connectivity and/or shared inputs that are reflected in the trial to trial variability of responses. Noise correlations were much higher for PV than for PC pairs (Fig. 5a,b, $P < 0.001$ for all comparisons). The magnitude of average noise correlations for each group of cell pairs was not different between the two visual stimulation protocols (Fig. 5a,b, $P > 0.3$ for all comparisons).

Comparing the pattern of noise correlations between different stimulus conditions to the pattern of spontaneous correlations allowed us to explore if the extensive restructuring of PC co-activations (Fig. 4h) arose primarily from changes in stimulus-evoked response patterns (signal correlation) or also from changes in the structure of noise correlation. For PCs, the pattern of pair-wise noise correlations in the population was relatively different from spontaneous correlation patterns for both stimulus conditions (Fig. 5c, group median pattern correlation spontaneous versus gratings = 0.37, spontaneous versus natural movie = 0.36), while for PV cells the pattern of noise correlations was more similar (Fig. 5c, group median pattern correlation spontaneous versus gratings = 0.66, spontaneous versus natural movie = 0.60). In fact, for both PC and PV cell populations the similarity of noise correlation patterns (Fig. 5c) was not significantly different from those obtained from total pair-wise correlations (compare to Fig. 4h, $P > 0.08$ for all comparisons).

For PCs, the differences in patterns of noise correlation and spontaneous correlation indicates that even the component of co-activation patterns that is not directly evoked by the visual stimulus is different from spontaneous co-activation patterns. Moreover, the structure of PC-PC noise correlations changed also between grating stimuli and natural movies (Fig. 5c, group median pattern correlation = 0.26), suggesting that different types of feedforward input not only regroup the local population of PCs into different ensembles, but also place the local circuit into very different activity states with changed network interactions. PV cells, in contrast, behaved differently: their co-activation patterns were largely maintained in the absence or presence of feedforward input.

Discussion

We found fundamental differences in synaptic connectivity, visual response properties and network dynamics between populations of layer 2/3 excitatory PCs and inhibitory PV/FS interneurons in mouse V1. Co-activations of sparsely but selectively connected PCs were strongly dependent on stimulus identity, and only weakly reflected biased local connectivity. In contrast, the pattern of co-activations of densely connected and more broadly tuned PV/FS cells was weakly dependent on visual input, and appeared to largely reflect local network activity.

The contribution of inhibition during sensory processing in V1 will crucially depend on the tuning properties of interneurons. There is considerable debate about the selectivity of PV/FS interneurons, which provide rapidly acting, soma-targeted inhibition of PCs[1,20–22]. We used cell-attached recordings and two-photon calcium imaging in mice expressing tdTomato in PV neurons, which mostly comprised FS cells, and found that their calcium

signals reliably reflected changes in firing rate. We found that PV/FS cells exhibited a range of tuning widths. While a small subset of cells was more selective for stimulus orientation, the great majority was more broadly tuned (Fig. 1). This result was additionally confirmed in both wild-type and PV-tdTomato mice by in vitro electrophysiological identification of FS cells, whose orientation tuning had been functionally characterized in vivo (Fig. 2).

The broader tuning of most PV/FS cells in mice is consistent with their synaptic connectivity profile in the local network. We found that FS interneurons received highly dense, local excitatory connections (see also ref. 23) that were on average an order of magnitude stronger than connections between PCs. We found this arrangement of PC-to-FS connections to be much denser than in rat visual cortex7, which may reflect either a difference between species or a consequence of fewer severed connections between neurons due to our recording deeper in the slice. Importantly, in combined *in vivo* and *in vitro* experiments on the same tissue, we have shown directly that predominantly broadly tuned PV/FS cells indiscriminately sample strong inputs from a local population of PCs with a diverse range of orientation preference and selectivity. Our data support the idea that local inhibition in V1 is recruited non-specifically and primarily reflects the strength of firing in the local network20, but argues against distinct subnetworks of excitatory and inhibitory neurons sharing the same preference for visual features10,22. Our results additionally provide a prediction for the width of orientation tuning of FS interneurons in carnivore V1 which, unlike in mice, contains functional columns: given similarly dense PC-FS connectivity, the tuning of FS neurons is expected to be narrow in iso-orientation domains, but broader in pinwheel centers, which may explain mixed reports regarding the selectivity of FS neurons in the cat16–18.

How do these fundamental differences in synaptic connectivity and feature selectivity of PCs and PV/FS cells relate to their network dynamics? Neuronal responses during sensory processing are likely to be influenced both by the intrinsic organization of intracortical connections and the statistical features of sensory stimuli that provide the main feedforward drive to the cortical circuit. The extent to which these intrinsic and extrinsic factors dominate cortical activity is still not resolved. On one hand, several reports suggest that patterns of evoked activity resemble those occurring spontaneously, and that the structure of neuronal correlations remains similar irrespective of the presence or absence of a sensory drive24–29. On the other hand, other studies report that sensory stimuli or changes in brain state can alter the strength of neuronal correlations and network interactions30–32,44–46. The different extents to which sensory input restructures patterns of cortical network activity as reported by different studies could be attributed to various factors other than cell type such as different animal species, cortical areas, cortical layer, and the spatial scale, coverage and resolution of the methods used. While our study cannot account for all these factors, our data make a clear distinction between the behavior of layer 2/3 PC and PV/FS cell assemblies.

In populations consisting of inhibitory PV/FS cells, correlations in both overall activity and trial-to-trial variability were similar during periods of spontaneous and visually evoked activity. This agrees with the very dense sampling of local excitatory connections by PV/FS cells, such that nearby PV cells share a substantial amount of common input, and are therefore more correlated than those separated by greater distances (Supplementary Fig. 5).

These results are also consistent with the observation that spontaneously occurring action potentials of neighboring FS cells in mouse somatosensory cortex are synchronized and are driven by highly correlated depolarizations44. Membrane potential synchronization may be additionally augmented by electrical coupling42,43. Therefore, the co-activation patterns of nearby PV/FS cells are not strongly altered by sensory drive. Instead this weak stimulus-dependence of PV/FS cell correlations is consistent with the notion that activity of these interneurons is largely dominated by local activity in the network. While neighboring PV/FS neurons may additionally receive selective feedforward or long-range excitatory connections, these inputs are apparently not sufficient to substantially de-correlate their firing (on the scale of 100s ms).

In populations of PCs, we found a very weak relationship between the similarity of visual responses (signal correlation) and the magnitude of spontaneous firing rate correlations, suggesting that neurons preferring similar visual features tended to be only slightly more co-active spontaneously. Importantly, the structure of both firing rate (total) and noise correlations was only weakly related between the spontaneous state and during presentation of drifting gratings and naturalistic movies, indicating that the same neuronal subsets were rarely similarly co-active during these conditions. These results suggest that the cortical representation of a visual stimulus in PC populations does not strongly reflect the existing biases of their recurrent connectivity. Since the connections between nearby PCs in layer 2/3 are both sparse and weak (Fig. 2), the fraction of shared local input between a pair of PCs is likely to be small, allowing feedforward or other inputs to influence and potentially decorrelate their firing. At present, however, it is not possible to identify the main sources of correlated variability of PCs beyond ruling out a dominant role of biased local connections, whose influence may be additionally attenuated by active mechanisms of decorrelation33,35. Our data support the idea that regrouping of PCs into different ensembles is strongly governed by the statistics of sensory input, which is in agreement with reports on state- or stimulus-dependence of neuronal interactions30–32,44,45.

These data reveal fundamentally different operational regimes of excitatory and inhibitory neurons during sensory processing. Similar patterns of co-activation of PV/FS cells across stimulus conditions contrasted with the strong dependence of PC co-activations on sensory drive whereby unique stimuli can be represented with unique PC response patterns. These attributes of PC activity may offer significant advantages for sensory coding, as, ensembles of PCs are much more informative about the identity of a stimulus than PV/FS cells (Supplementary Fig. 9). Thus, in a sparsely active local network composed of PCs with diverse receptive fields, the variability and independence of responses may act to reduce local activity correlations and improve the efficiency of population coding34,47.

Methods

Animals and Surgical Procedures

All experimental procedures were carried out in accordance with institutional animal welfare guidelines and licensed by the UK Home Office. Experiments were performed on C57Bl/6 mice or PV-Cre x lsl-tdTomato transgenic mice. Generation and characterization of the PV-Cre-lsl-tdTomato transgenic mouse line was described previously (original name: Pvalb-2A-

Cre;Ai939). Briefly, the PV-Cre mouse line was generated by constructing a targeting vector in which the T2A-Cre sequence was fused in-frame to the 3' end of the PV coding sequence, transfecting the targeting vector into the G4 129/B6 F1 hybrid ES cell line, and selecting properly recombined ES clones to produce the mouse line. The PV-Cre mice were then crossed with the Ai9 lsl-tdTomato reporter line39 to produce the double transgenic PV-Cre-lsl-tdTomato mice for experiments.

Mice were initially anesthetized with a mixture of Fentanyl (0.05 mg/kg), Midazolam (5.0 mg/kg), and Medetomidin (0.5 mg/kg). At the time of imaging, the injectable anesthetic had mostly worn off and light anesthesia was maintained by isoflurane (0.3 -0.5%) in a 60:40% mixture of O_2:N_2O delivered via a small nose cone. Surgery was performed as described previously38. Briefly, a small craniotomy (1-2mm) was carried out over primary visual cortex and sealed after dye injection with 1.6% Agarose in Hepes-buffered ACSF and a cover slip.

Dye Loading and two-photon Imaging

For bulk loading of cortical neurons36 the calcium-sensitive dye Oregon Green Bapta-1 AM (OGB-1 AM, Molecular Probes) was first dissolved in 4 µl DMSO containing 20% Pluronic F-127 (Molecular Probes), and further diluted (1/11) in dye buffer (150 mM NaCl, 2.5 mM KCl, and 10 mM HEPES [pH 7.4]) to yield a final concentration of 0.9 mM. Sulforhodamine 101 (50µM, Molecular Probes) was added to the solution for experiments in C57Bl/6 mice to distinguish neurons and astrocytes48. The dye was slowly pressure injected into the right visual cortex at a depth of 170-200 µm with a micropipette (3–5 MΩ, 3-10 psi, 2–4 min) under visual control by two-photon imaging (10× water immersion objective, Olympus). Activity of cortical neurons was monitored by imaging fluorescence changes with a custom-built microscope and a mode-locked Ti:sapphire laser (Mai Tai, Spectra-Physics) at 830 nm or 930 nm through a 40× water immersion objective (0.8 NA, Olympus). Scanning and image acquisition were controlled by custom software written in LabVIEW (National Instruments).

In vivo cell-attached recordings

Loose-seal cell-attached recordings *in vivo* were performed on OGB-1 loaded neurons in layer 2/3 with micropipettes of 4-7 MΩ, pipette solution containing (in mM): 150 NaCl, 2.5 KCl, 10 Hepes, 1 MgCl2, 1 CaCl2 (300mOsm) and 25 µM Alexa Fluor 594. The craniotomy was covered with agar. Neurons were targeted visually with two-photon imaging at 830 or 930 nm. Signals were recorded using a ELC-03XS amplifier (NPI) and Igor Pro NClamp/ Neuromatic software (Jason Rothman, UCL), band-pass filtered between 0.3 and 5 kHz and digitized at 10kHz.

Visual Stimulation

Visual stimuli were generated using MATLAB (Mathworks) Psychophysics Toolbox49, and displayed on a LCD monitor (60 Hz refresh rate) positioned 20 cm from the left eye, roughly at 45 degree to the long axis of the animal, covering ˜105×85 degrees of visual space. At the beginning of each experiment, the appropriate retinotopic position in visual cortex was determined using small grating stimuli at 12-24 neighboring positions. Only cortical regions

in the monocular part of primary visual cortex were included in the analysis. The monitor was repositioned such that the preferred retinotopic position of most imaged neurons was roughly in the middle of the monitor. Calcium signals were measured in the dark (monitor and room lights turned off) for 6-12 minutes, and in response to sequences of full-field grating stimuli and natural movies. Square wave gratings (0.035 cycles/°, 2 cycles/s) drifting in eight different directions were shown episodically at 100% contrast, with the grating standing for 4 s (occasionally, a grey screen was used instead of the standing grating) before moving for 2 s (8 stimulus repetitions). Naturalistic movies consisted of 16 s sequences of either moving scenes in a mouse cage or compilations of David Attenborough's Life of Mammals (BBC), adjusted to 70% mean contrast, continuously looped 19 times. The first stimulus repetition was removed from analysis to exclude onset-related responses. For the functional characterization of neurons prior to *in vitro* connectivity mapping, square wave gratings drifting in eight different directions were randomly interleaved, with the grating standing for 1.4-1.9 s before moving for 0.9-1.5 s (6-8 repetitions per grating).

Data Acquisition and Analysis

Imaging frames of 256×256 pixels or 256×128 pixels were acquired at 7.6 or 15.2 Hz, respectively. Image sequences recorded at 15.2 Hz were subsequently re-sampled to 7.6 Hz. After each recording the focal plane and imaging position was checked and realigned with the initial image if necessary. Image sequences were aligned for tangential drift and analyzed with custom programs written in ImageJ (NIH), MATLAB and LabVIEW. Cell outlines were detected using a semi-automated algorithm based on cell intensity, size, and shape, and confirmed by visual inspection. After erosion of the cell-based regions of interest (ROIs) (to minimize influence of the neuropil signal around the cell bodies) all pixels within each ROI were averaged to give a single time course (ΔF/F), which was additionally high-pass filtered at a cut-off frequency of 0.02 Hz to remove slow fluctuations in the signal. Non-responsive neurons were excluded from further analysis, by testing whether, for each cell, a significant calcium response was observed relative to baseline for at least one grating direction and for one or more frames of the natural movie sequence (one-way ANOVA, $P < 0.0001$).

For determining neuronal response preferences to drifting gratings from average responses for *in vivo* to *in vitro* connectivity mapping experiments, spike trains were inferred from calcium signals using a fast non-negative de-convolution method which approximates the most likely spike train for each neuron, given the fluorescence observations40. This method yields spike probabilities that approximate the number of action potentials per imaging frame, or inferred firing rate. For pyramidal neurons, τ (decay constant of calcium transients) was set to 0.8 s, and calcium signal baseline was the mean of all values from the calcium trace. For PV-positive or fast-spiking neurons τ was set to 2 s, and the baseline was determined as the 10^{th} percentile of all values. These settings resulted in the best correspondence between inferred spike probability and real spike rate measured during simultaneous calcium imaging and cell-attached recordings (Supplementary Fig. 2 and 4, 16 pyramidal cells from 7 mice, 12 PV cells from 6 mice). We found that for pyramidal neurons inferred spike probabilities of 0.022 or less, and for PV cells probabilities of 0.008 or less, were typically not associated with actual spikes, and were therefore set to 0. To relate

inferred spiking probability to actual spike rate for pyramidal neurons (Supplementary Fig. 2f) empirically recorded spikes were attributed to inferred spiking values if they occurred with a time difference Δt of less than 195 ms and were not already assigned to a previous inferred spike. The average calcium signal from the same time window shifted by one bin was taken to compare calcium transient amplitude and real spike rate (Supplementary Fig. 2e). The algorithm detected 100% of bursts of three or more spikes, 95 ± 2 % (Mean ± SEM) of bursts of two spikes, and 53 ± 6 % of single spikes, with a false-positive rate of 0.049 ± 0.009 Hz. Since PV cells showed on average much higher spike rates, spikes were not attributed to inferred spikes, but inferred spiking values or real spikes were summed, and the calcium signal averaged in time bins of 393 ms for comparison (Fig. 1d,e, Supplementary Fig. 4c,d). For PV cells the algorithm detected 92 ± 2 % of all spikes with a false-positive rate of 0.25 ± 0.03 Hz. Since spike rates were much higher for PV cells than for pyramidal cells (average spike rate during stimulation with episodically drifting gratings for pyramidal neurons: 0.57 ± 0.09 Hz; PV neurons: 8.2 ± 1.8 Hz), false positive rates as a fraction of total spike count were roughly similar for the two cell types.

Among cells responsive to grating stimuli, the average firing rate, average inferred firing rate or the average calcium signal over the duration of grating drift was taken as the response to each grating stimulus. Responses from different trials were averaged to obtain the orientation tuning curve. This orientation tuning curve was then Fourier interpolated to 360 points, and the preferred direction was determined by the angle at which the interpolated tuning curve attained its maximum. The preferred orientation was taken as the modulus of the preferred direction to 180 degrees. Orientation selectivity index (OSI) was calculated as $(R_{best}-R_{ortho})/(R_{best}+R_{ortho})$, where R_{best} is the interpolated response to the best direction, and R_{ortho} is the average of interpolated responses to the directions orthogonal to best responding direction.

Correlations, Pattern correlations and matrix reordering

Pair-wise correlations were calculated using Pearson's correlation coefficient from calcium signals of two cells over the duration of the whole recording (total correlation). Signal correlation was calculated from average responses across trials of drifting gratings or natural movies, and noise correlations were determined by subtracting the average response from the responses in each trial and calculating the correlation coefficient of the mean-subtracted response over the time course of the recording. For Figure 3d, correlation coefficients of all cell pairs from each imaged region were first z-scored (each value was normalized by subtracting the population mean and dividing by the variance), before pooling the data from all the regions in a single plot.

For visual comparison, the correlation coefficients were displayed in matrix form (Fig. 4g), whereby each element is the correlation coefficient for a pair of neurons. Neurons were ordered such that the strongest values were close to the diagonal for one stimulus condition; we used a search algorithm in order to maximize the Frobenius inner product between the actual pairwise correlation matrix and a Toeplitz matrix whose values decay exponentially from the diagonal28. In order to aid direct visual comparison, this ordering was applied to

the correlation matrices of other conditions. The similarity between two matrices (pattern correlation) is the correlation coefficient of their off-diagonal elements.

Immunocytochemical and Electrophysiological characterization of layer 2/3 PV neurons

For immunocytochemical analysis transgenic animals were perfused with 4% paraformaldehyde in PBS and 50 μm-thick coronal slices were obtained from the visual cortex. Free-floating sections were incubated (4°C, 48 hours) in PBS and Triton X-100 (0.2% v/v) solution containing primary antibodies against parvalbumin (mouse anti-PV, 1:1000, Swant #PV235, Switzerland). Fluorescent conjugates were used to visualize PV immunoreactivity (AlexaFluor 488-conjugated goat anti-mouse, 1:1000, 4°C, overnight, Invitrogen, California). Primary and secondary antibodies were initially tested for optimal dilution. Mounted sections were analyzed using two-photon scanning microscopy at 930nm wavelength, with a filter set suitable for separating AlexaFluor 488 and tdTomato fluorescence emission. In superficial layers (< 200 μm from the pial surface), which correspond to the regions recorded during in vivo calcium imaging, tdTomato was coexpressed with parvalbumin in 92 % of the tdTomato-expressing cells (88 out of 96) and in 100 % of the parvalbumin-positive cells (Supplementary Fig. 1f, top and middle panels). In deeper layers, however, the co-localisation was poorer (Supplementary Fig. 1f, bottom panels), possibly due to expression of PV in some layer 5 pyramidal neurons during development50.

Three adult PV-Cre-lsl-tdTomato mice were used for electrophysiological characterization of PV neurons. The mouse brain was removed and dissected rapidly in ice-cold artificial cerebrospinal fluid (ACSF) containing (in mM) 125 NaCl, 2.5 KCl, 1 $MgCl_2$, 1.25 NaH_2PO_4, 2 $CaCl_2$, 26 $NaHCO_3$, 25 Dextrose; osmolarity 315-325 mOsm, bubbled with 95% O_2/5% CO_2, pH 7.4. Visual cortex slices (300 μm) were cut coronally (HM 650 V Vibration Microtome, MICROM) and incubated at 34 °C for thirty minutes before they were transferred to the recording chamber. Recording pipettes were filled with (in mM): 5 KCl, 115 K-Gluconate, 10 K-HEPES, 4 Mg-ATP, 0.3 Na-GTP, 10 Na-Phosphocreatine; 40 μM Alexa Fluor 594 and 0.1% w/v Biocytin; 290–295 mOsm, pH 7.2. The chloride reversal potential was ˜-85.2 mV. Liquid junction potential was not corrected for. Cells were approached under visual guidance using laser-scanning Dodt contrast imaging, and simultaneous two-photon imaging allowed detection of fluorescence from tdTomato-expressing cells. Whole-cell recordings were carried out in 32 °C ACSF, using Multiclamp 700b amplifiers (Axon Instruments) and custom software running on IGOR Pro (WaveMetrics Inc.). Step currents from -200/-100/-50 pA to 700/350/175 pA at 50/25/12.5 pA increments were injected to determine I-V relationship. Spike threshold was measured from the inflexion point of the minimally suprathreshold trace. Spike height was the difference between spike threshold and peak. Spike half-width was measured at the mean of threshold and peak. Cells were classified according to firing pattern1 (Supplementary Fig. 1a-e). For accurate measurement of spike parameters, cells were included only if the series resistance was less than 30 MΩ.

In vitro mapping of connectivity between neurons functionally characterized *in vivo*

Connectivity mapping experiments were performed both in C57Bl/6 mice (8 FS cells) and PV-Cre x lsl-tdTomato transgenic mice (11 PV cells) as described before11. Briefly, after vivo two-photon calcium imaging of visual responses, small volumes of red fluorescent microspheres (Lumafluor, Florida) were injected into the imaged region to facilitate identification of the region in the coronally sliced brain. Whole-cell recordings from up to four cells simultaneously were carried out in the vicinity of the microsphere tract. The presence of synaptic connections was tested by evoking five spikes at 30-Hz in each cell, repeated 30-90 times. Paired-pulse ratio (PPR) was calculated as the amplitude of the second evoked EPSP over that of the first one. After connectivity mapping, step currents were injected to obtain I-V relationship. Cells were classified according to firing pattern and spike shape1. Out of 19 PV/FS interneurons patched whose responses were characterized in vivo (of which 17 were significantly responsive to drifting gratings), 5 were classic non-accommodating, 5 were delayed classic non-accommodating, 4 were accommodating, and IV curve was not obtained for 5 cells (lost after connectivity mapping). To match the same neurons imaged *in vivo* and recorded from *in vitro*, we performed three-dimensional image registration of *in vivo* and *in vitro* image stacks by affine transformation subsequent to the experiment. To relate connectivity to functional properties, the asymptotic Cochran-Armitage test for trend was used to test for significance.

Supplementary Material

Refer to Web version on PubMed Central for supplementary material.

Acknowledgements

We thank Troy Margrie, Alexander Arenz and Ede Rancz for help with *in vivo* electrophysiology, Jesper Sjöström and Kate Buchanan for help with *in vitro* electrophysiology, and Jason Rothman for providing NeuroMatic software. We thank Mark Hübener and Maneesh Sahani for comments on an earlier version of this manuscript. This work was supported by the Wellcome Trust (TMF), European Research Council (TMF), the European Molecular Biology Organization (SBH) and Humboldt Foundation (SBH). The research leading to these results has also received funding from the European Community's Seventh Framework Programme (FP2007-2013) under grant agreement no. 223326 (TMF).

References

1. Markram H, et al. Interneurons of the neocortical inhibitory system. Nat Rev Neurosci. 2004; 5:793–807. [PubMed: 15378039]
2. Gonchar Y, Wang Q, Burkhalter A. Multiple distinct subtypes of GABAergic neurons in mouse visual cortex identified by triple immunostaining. Front Neuroanat. 2007; 1:3. [PubMed: 18958197]
3. Sillito AM. The contribution of inhibitory mechanisms to the receptive field properties of neurones in the striate cortex of the cat. J Physiol (Lond.). 1975; 250:305–329. [PubMed: 1177144]
4. Priebe NJ, Ferster D. Inhibition, Spike Threshold, and Stimulus Selectivity in Primary Visual Cortex. Neuron. 2008; 57:482–497. [PubMed: 18304479]
5. Ozeki H, Finn IM, Schaffer ES, Miller KD, Ferster D. Inhibitory stabilization of the cortical network underlies visual surround suppression. Neuron. 2009; 62:578–592. [PubMed: 19477158]
6. Liu B, et al. Intervening inhibition underlies simple-cell receptive field structure in visual cortex. Nat Neurosci. 2010; 13:89–96. [PubMed: 19946318]
7. Holmgren C, Harkany T, Svennenfors B, Zilberter Y. Pyramidal cell communication within local networks in layer 2/3 of rat neocortex. J Physiol. 2003; 551:139–153. [PubMed: 12813147]

8. Thomson AM, Lamy C. Functional maps of neocortical local circuitry. Front Neurosci. 2007; 1:19–42. [PubMed: 18982117]
9. Oswald A-MM, Doiron B, Rinzel J, Reyes AD. Spatial profile and differential recruitment of GABAB modulate oscillatory activity in auditory cortex. J Neurosci. 2009; 29:10321–10334. [PubMed: 19692606]
10. Yoshimura Y, Callaway EM. Fine-scale specificity of cortical networks depends on inhibitory cell type and connectivity. Nat Neurosci. 2005; 8:1552–1559. [PubMed: 16222228]
11. Ko H, et al. Functional specificity of local synaptic connections in neocortical networks. Nature. 2011; doi: 10.1038/nature09880
12. Yoshimura Y, Dantzker JLM, Callaway EM. Excitatory cortical neurons form fine-scale functional networks. Nature. 2005; 433:868–873. [PubMed: 15729343]
13. Gilbert CD, Wiesel TN. Columnar specificity of intrinsic horizontal and corticocortical connections in cat visual cortex. J Neurosci. 1989; 9:2432–2442. [PubMed: 2746337]
14. Alonso JM, Usrey WM, Reid RC. Rules of connectivity between geniculate cells and simple cells in cat primary visual cortex. J Neurosci. 2001; 21:4002–4015. [PubMed: 11356887]
15. Alonso JM, Martinez LM. Functional connectivity between simple cells and complex cells in cat striate cortex. Nat Neurosci. 1998; 1:395–403. [PubMed: 10196530]
16. Hirsch JA, et al. Functionally distinct inhibitory neurons at the first stage of visual cortical processing. Nat Neurosci. 2003; 6:1300–1308. [PubMed: 14625553]
17. Cardin JA, Palmer LA, Contreras D. Stimulus feature selectivity in excitatory and inhibitory neurons in primary visual cortex. J Neurosci. 2007; 27:10333–10344. [PubMed: 17898205]
18. Nowak LG, Sanchez-Vives MV, McCormick DA. Lack of orientation and direction selectivity in a subgroup of fast-spiking inhibitory interneurons: cellular and synaptic mechanisms and comparison with other electrophysiological cell types. Cereb Cortex. 2008; 18:1058–1078. [PubMed: 17720684]
19. Sohya K, Kameyama K, Yanagawa Y, Obata K, Tsumoto T. GABAergic neurons are less selective to stimulus orientation than excitatory neurons in layer II/III of visual cortex, as revealed by in vivo functional Ca2+ imaging in transgenic mice. J Neurosci. 2007; 27:2145–2149. [PubMed: 17314309]
20. Kerlin AM, Andermann ML, Berezovskii VK, Reid RC. Broadly tuned response properties of diverse inhibitory neuron subtypes in mouse visual cortex. Neuron. 2010; 67:858–871. [PubMed: 20826316]
21. Ma, W-pei; , et al. Visual representations by cortical somatostatin inhibitory neurons--selective but with weak and delayed responses. J Neurosci. 2010; 30:14371–14379. [PubMed: 20980594]
22. Runyan CA, et al. Response features of parvalbumin-expressing interneurons suggest precise roles for subtypes of inhibition in visual cortex. Neuron. 2010; 67:847–857. [PubMed: 20826315]
23. Bock DD, et al. Network anatomy and in vivo physiology of visual cortical neurons. Nature. 2011; 471:177–182. [PubMed: 21390124]
24. Tsodyks M, Kenet T, Grinvald A, Arieli A. Linking spontaneous activity of single cortical neurons and the underlying functional architecture. Science. 1999; 286:1943–1946. [PubMed: 10583955]
25. Ch'ng YH, Reid RC. Cellular imaging of visual cortex reveals the spatial and functional organization of spontaneous activity. Front Integr Neurosci. 2010; 4
26. Fiser J, Chiu C, Weliky M. Small modulation of ongoing cortical dynamics by sensory input during natural vision. Nature. 2004; 431:573–578. [PubMed: 15457262]
27. MacLean JN, Watson BO, Aaron GB, Yuste R. Internal dynamics determine the cortical response to thalamic stimulation. Neuron. 2005; 48:811–823. [PubMed: 16337918]
28. Luczak A, Barthó P, Harris KD. Spontaneous events outline the realm of possible sensory responses in neocortical populations. Neuron. 2009; 62:413–425. [PubMed: 19447096]
29. Jermakowicz WJ, Chen X, Khaytin I, Bonds AB, Casagrande VA. Relationship between spontaneous and evoked spike-time correlations in primate visual cortex. J Neurophysiol. 2009; 101:2279–2289. [PubMed: 19211656]
30. Smith MA, Kohn A. Spatial and temporal scales of neuronal correlation in primary visual cortex. J Neurosci. 2008; 28:12591–12603. [PubMed: 19036953]

31. Kohn A, Smith MA. Stimulus dependence of neuronal correlation in primary visual cortex of the macaque. J Neurosci. 2005; 25:3661–3673. [PubMed: 15814797]
32. Nauhaus I, Busse L, Carandini M, Ringach DL. Stimulus contrast modulates functional connectivity in visual cortex. Nat Neurosci. 2009; 12:70–76. [PubMed: 19029885]
33. Renart A, et al. The Asynchronous State in Cortical Circuits. Science. 2010; 327:587–590. [PubMed: 20110507]
34. Ecker AS, et al. Decorrelated Neuronal Firing in Cortical Microcircuits. Science. 2010; 327:584–587. [PubMed: 20110506]
35. Ohiorhenuan IE, et al. Sparse coding and high-order correlations in fine-scale cortical networks. Nature. 2010; 466:617–621. [PubMed: 20601940]
36. Stosiek C, Garaschuk O, Holthoff K, Konnerth A. In vivo two-photon calcium imaging of neuronal networks. Proc Natl Acad Sci USA. 2003; 100:7319–7324. [PubMed: 12777621]
37. Ohki K, Chung S, Ch'ng YH, Kara P, Reid RC. Functional imaging with cellular resolution reveals precise micro-architecture in visual cortex. Nature. 2005; 433:597–603. [PubMed: 15660108]
38. Mrsic-Flogel TD, et al. Homeostatic Regulation of Eye-Specific Responses in Visual Cortex during Ocular Dominance Plasticity. Neuron. 2007; 54:961–972. [PubMed: 17582335]
39. Madisen L, et al. A robust and high-throughput Cre reporting and characterization system for the whole mouse brain. Nat Neurosci. 2010; 13:133–140. [PubMed: 20023653]
40. Vogelstein JT, et al. Fast nonnegative deconvolution for spike train inference from population calcium imaging. J Neurophysiol. 2010; 104:3691–3704. [PubMed: 20554834]
41. Niell CM, Stryker MP. Highly Selective Receptive Fields in Mouse Visual Cortex. J Neurosci. 2008; 28:7520–7536. [PubMed: 18650330]
42. Galarreta M, Hestrin S. A network of fast-spiking cells in the neocortex connected by electrical synapses. Nature. 1999; 402:72–75. [PubMed: 10573418]
43. Gibson JR, Beierlein M, Connors BW. Two networks of electrically coupled inhibitory neurons in neocortex. Nature. 1999; 402:75–79. [PubMed: 10573419]
44. Gentet LJ, Avermann M, Matyas F, Staiger JF, Petersen CCH. Membrane Potential Dynamics of GABAergic Neurons in the Barrel Cortex of Behaving Mice. Neuron. 2010; 65:422–435. [PubMed: 20159454]
45. Zohary E, Shadlen MN, Newsome WT. Correlated neuronal discharge rate and its implications for psychophysical performance. Nature. 1994; 370:140–143. [PubMed: 8022482]
46. Poulet JFA, Petersen CCH. Internal brain state regulates membrane potential synchrony in barrel cortex of behaving mice. Nature. 2008; 454:881–885. [PubMed: 18633351]
47. Chelaru MI, Dragoi V. Efficient coding in heterogeneous neuronal populations. Proc Natl Acad Sci U S A. 2008; 105:16344–16349. [PubMed: 18854413]
48. Nimmerjahn A, Kirchhoff F, Kerr JND, Helmchen F. Sulforhodamine 101 as a specific marker of astroglia in the neocortex in vivo. Nat Methods. 2004; 1:31–37. [PubMed: 15782150]
49. Brainard DH. The Psychophysics Toolbox. Spat Vis. 1997; 10:433–436. [PubMed: 9176952]
50. Tanahira C, et al. Parvalbumin neurons in the forebrain as revealed by parvalbumin-Cre transgenic mice. Neurosci Res. 2009; 63:213–223. [PubMed: 19167436]

Europe PMC Funders Author Manuscripts

Europe PMC Funders Author Manuscripts

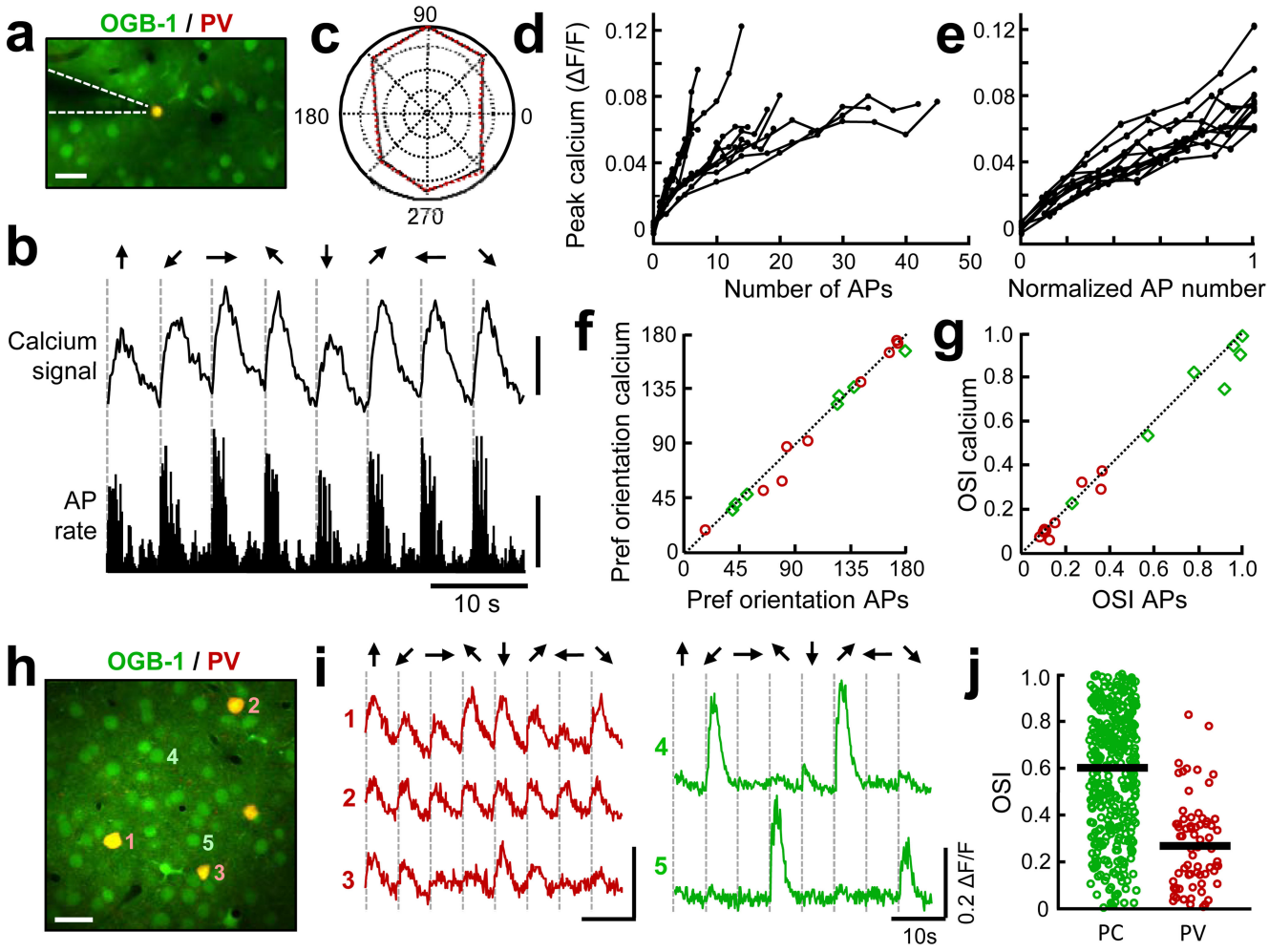

Figure 1. Calcium imaging and electrophysiological recordings of visually evoked responses in Parvalbumin (PV)-expressing neurons.

a. Image of an OGB-1 labeled PV-positive (PV) neuron in a Cre-PV-lsl-tdTomato mouse from which a cell-attached recording was made. Scale bar, 20 μm **b.** Average calcium signal (ΔF/F, top) and action potential (AP) rate per imaging frame (bottom) from simultaneous calcium imaging and electrophysiological recording from a PV neuron during stimulation with drifting gratings. Scale bars, 5% ΔF/F, 4 spikes per bin, bin size 131 ms. The directions of drifting gratings are indicated on top, dashed lines show drift onset. **c.** Polar plot of normalized responses to different grating directions from neuron in **b**, calculated from APs (black solid line) and calcium signal (red dashed line). **d, e.** Average peak calcium signal plotted against absolute AP number (**d**) or against normalized AP number (normalized to maximum number of APs) (**e**) for each of 12 PV neurons from 6 mice, calculated for bins of 393 ms. Error bars are omitted for clarity. **f, g.** Correspondence of preferred grating orientation (**f**) and orientation selectivity index (OSI, see methods) (**g**) calculated from calcium signal and from APs for 9 PV neurons (red circles) and 7 PCs (green diamonds) that were visually stimulated and responsive to moving gratings. **h.** Image of OGB-1 AM labeled tissue, including four PV neurons (red) in layer 2/3. Scale bar, 20 μm **i**. Average calcium

traces (ΔF/F) from three PV (red, left) and two PV-negative neurons (putative PCs, green, right) during stimulation with episodically presented drifting gratings (8 directions, 6 repetitions). The directions of drifting gratings are indicated on top, dashed lines show drift onset. **j.** Orientation selectivity index (OSI) for PCs (green) and PV interneurons (red), which significantly responded to grating stimuli (ANOVA, $P < 0.0001$). OSI for highly-selective, sharply-tuned neurons approaches 1, whereas OSI for broadly-tuned, non-selective neurons approaches zero. Black lines indicate median OSI. PC: median OSI = 0.60, PV: median OSI = 0.26; 15 regions, 7 animals, $P < 10^{-6}$).

Europe PMC Funders Author Manuscripts

Europe PMC Funders Author Manuscripts

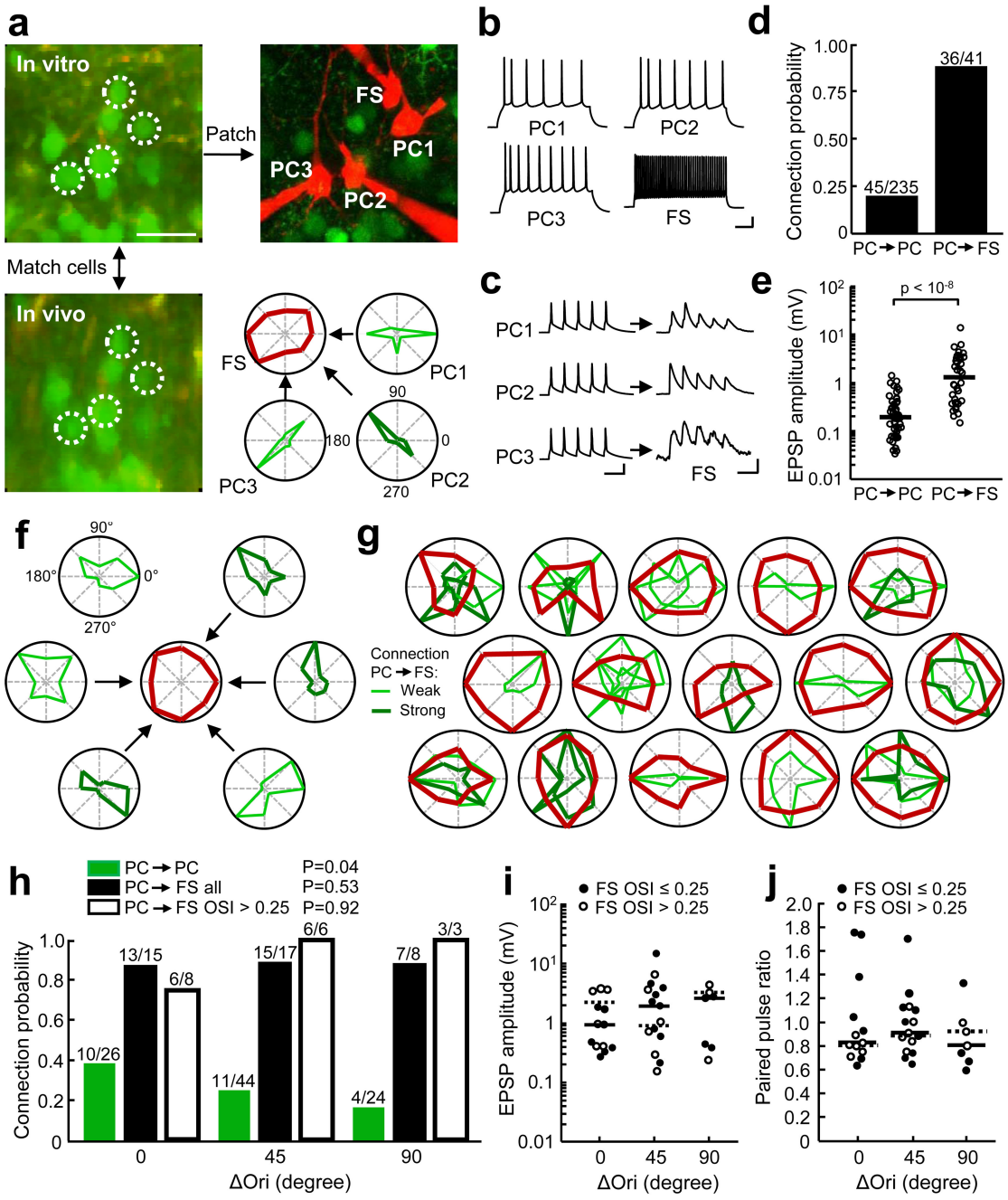

Figure 2. Assessing synaptic connectivity in vitro between neurons functionally characterized in vivo.

a. Images of OGB-1 labeled V1 tissue in a slice (top, left) and of the same cells in vivo before slicing (bottom, left, after registration of the image stacks, see Methods), white circles denote matched neurons *in vivo* and *in vitro,* which were targeted for whole-cell recording and filled with Alexa 594 (top, right). Three pyramidal cells (PCs) and one fast-spiking interneuron (FS) were patched. Bottom, right: Polar plots of normalized responses to gratings drifting in 8 different directions, illustrating their orientation/direction preference and tuning. **b.** Action potential firing pattern in response to depolarizing current injection for

the cells from **a**. Scale bars: 20 mV, 50 ms. **c.** Average traces of postsynaptic potentials in the FS interneuron in response to spike-evoking current injections in each of the three PCs from **a**, showing that all three were providing synaptic input onto the FS neuron. Scale bars: left panel: 40 mV, 50 ms; right panel: 2 mV for upper two traces, 0.2 mV for bottom trace; 50 ms. **d.** Probability of finding synaptic connections between pairs of PCs and from PC to PV/FS neurons. **e.** Amplitudes of excitatory postsynaptic potentials (EPSPs) between PCs and from PCs to PV/FS cells. Black lines depict median amplitudes. **f.** Another example of connectivity between six PCs and one PV/FS interneuron and their orientation preferences. Five out of the six PCs provided input onto the PV/FS neuron, which was held in whole-cell mode continuously while two sets of three PCs were patched and their connectivity assayed sequentially. **g.** Polar plots with normalized responses to drifting grating stimuli (8 directions) of 15 additional visually-responsive PV/FS interneurons (red lines) overplotted with normalized responses of the PCs that were found to provide synaptic input onto them (green lines). PCs which provided stronger connections (> 2mV EPSP amplitude) are indicated by darker and thicker green lines. **h.** Relationship between connection probability and difference of preferred orientation (ΔOri) for pairs of orientation-tuned (OSI > 0.4) PCs (green), from PCs to PV/FS interneurons (black, filled bars) and from PCs to PV/FS interneurons with OSI > 0.25 (black, open bars). Two PCs were more likely to be connected if they preferred similar grating orientations. Connection probability from PC onto PV/FS cells was not dependent on response similarity, irrespective of response selectivity. **i.** Connection strength (EPSP amplitude) from PCs to PV/FS cells plotted against difference in preferred orientation of each cell pair (ΔOri). Closed circles, pairs with OSI ≤ 0.25; open circles, pairs with OSI > 0.25. Strength of input was not dependent of orientation preference similarity: all cell pairs, P = 0.59, only cell pairs with OSI > 0.25, P = 0.94, Kruskal-Wallis test. **j.** Relationship between paired-pulse ratio of synaptic connections from PCs to PV/FS cells and ΔOri. Degree of facilitation (PPR>1) or depression (PPR<1) of synapses was not related to response similarity to gratings: all cell pairs, P = 0.54, only cell pairs with OSI > 0.25, P = 0.11, Kruskal-Wallis test. Black lines depict median amplitudes, dotted lines median amplitudes for pairs with OSI > 0.25. Bins include difference in preferred orientation values of 0 to 22.5° (zero degree bin), 22.5° to 67.5° (45 degree bin), and 67.5° to 90° (90 degree bin).

Europe PMC Funders Author Manuscripts

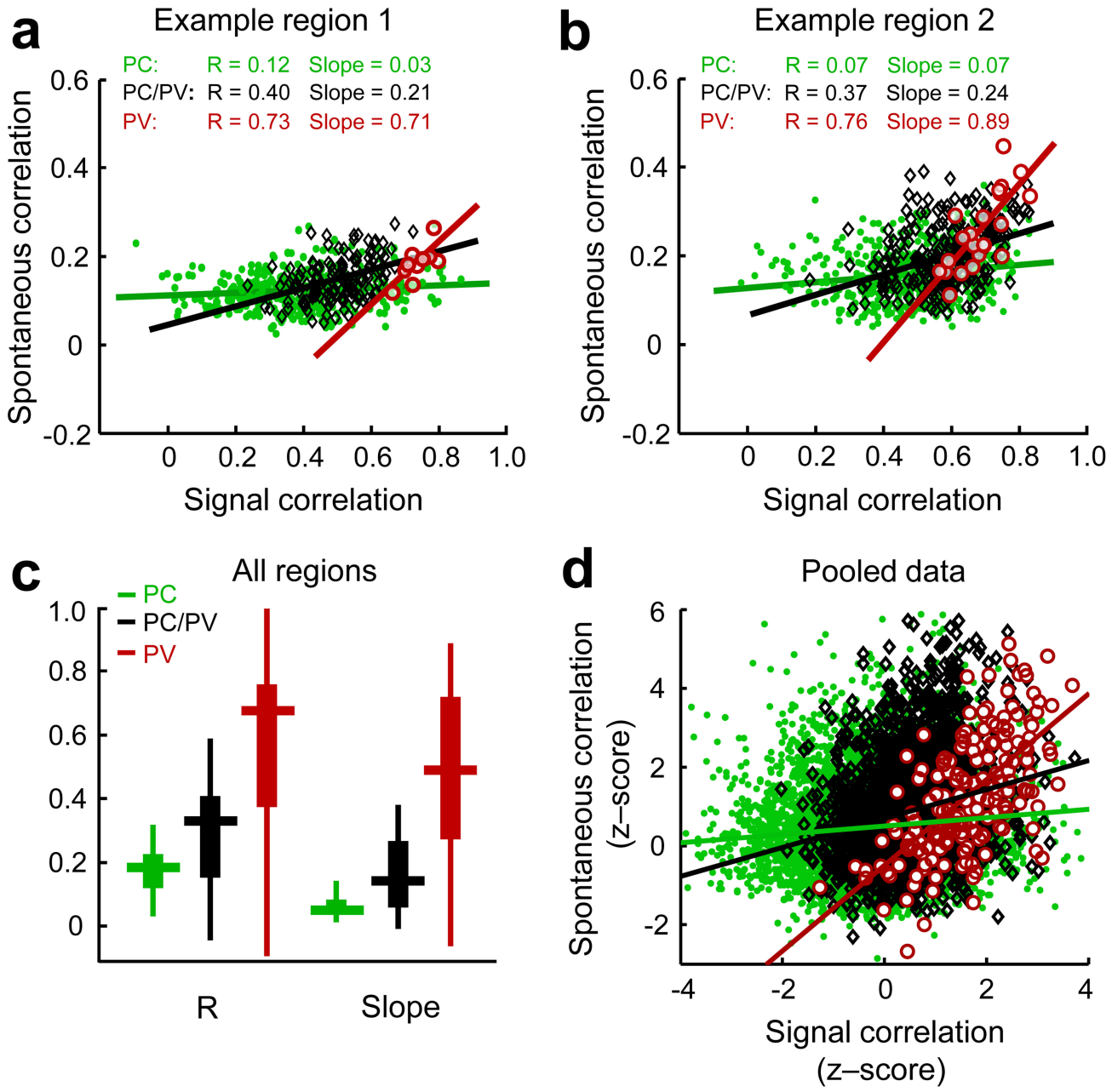

Figure 3. Relationship between response similarity and pair-wise correlations during spontaneous activity.

a,b. Spontaneous pair-wise correlation coefficients plotted against pair-wise signal correlation coefficients (obtained from averaged responses to gratings drifting in eight different directions) from two different imaging regions, for pairs of PV-negative neurons (PC, green), mixed pairs of one PC and one PV-positive (PV) neuron (black), and pairs of PV neurons (red). **c.** Boxplots of the correlation coefficients (R) and slopes of the relationship between spontaneous correlations and signal correlations from all imaged regions. **d.** Pooled data from all PC pairs (green), mixed pairs (black) and PV cell pairs (red) normalized for comparison across animals and imaged regions by computing z-scores (see

Methods). PC-pairs: R = 0.10, slope = 0.11; PC/PV-pairs: R = 0.22, slope = 0.37; PV-pairs: R = 0.61, slope = 1.08. 15 regions, 7 animals, 7285 PC cell pairs, 2562 PC/PV cell pairs, 187 PV cell pairs.

Europe PMC Funders Author Manuscripts

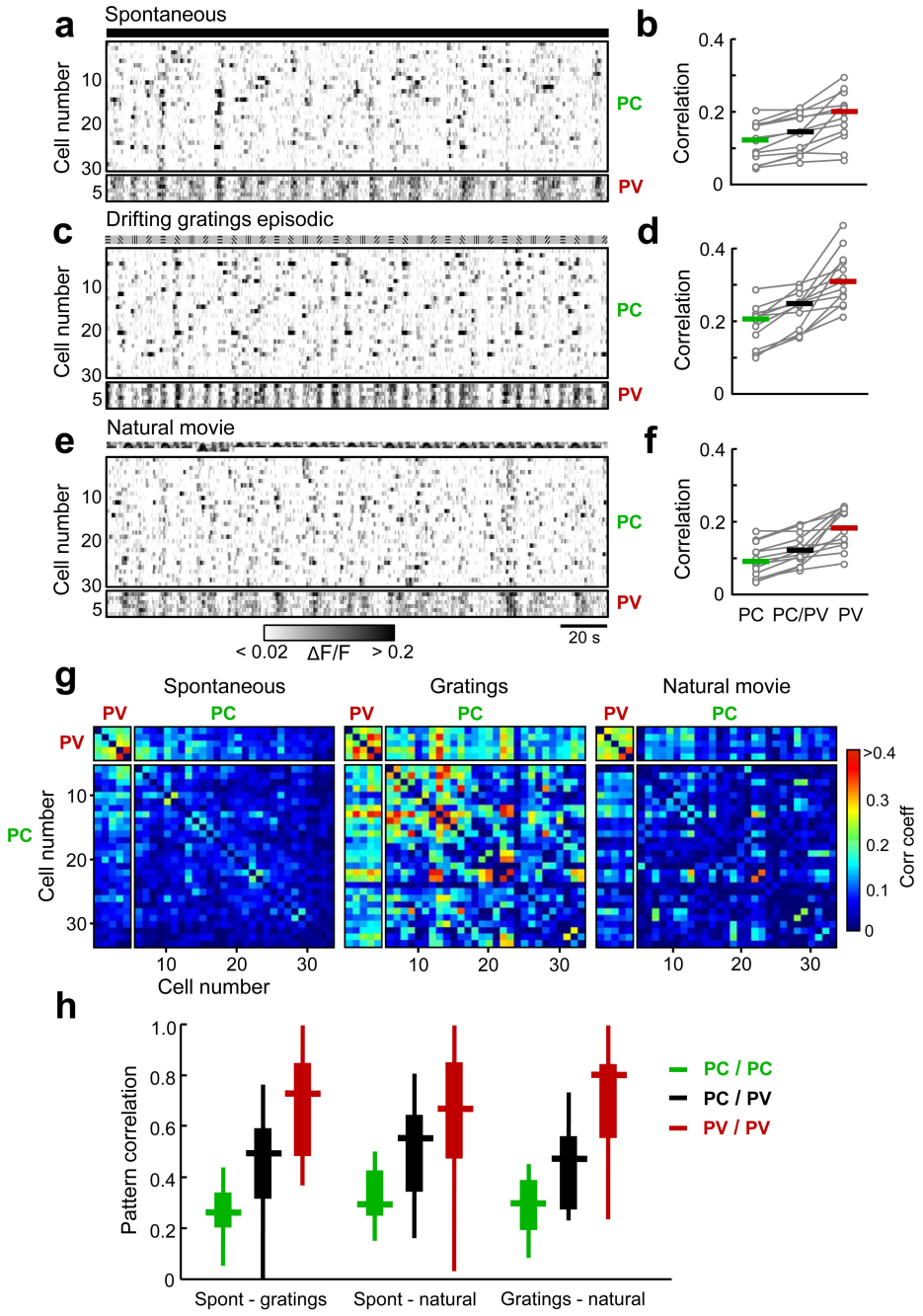

Figure 4. Comparison of population activity patterns with and without visual stimulation.

a,c,e. Calcium signals of 30 PC (top) and 6 PV (bottom) neurons simultaneously imaged in darkness with the monitor switched off (**a**), and during stimulation with episodically drifting gratings (**c**), or with natural movie sequences (**e**). Schematic stimulus sequence is shown above each plot. **b,d,f.** Strength of pair-wise time-varying (total) correlations from calcium signals for PC pairs (left), PV pairs (right) and mixed PC/PV pairs (middle) during spontaneous activity (**b**), and during visual stimulation with gratings (**d**), or natural movies (**f**). Circles depict median values of each imaged region, colored lines indicate group

median. Grey lines connect values obtained from the same imaged region. **g.** Matrices of pair-wise response rate correlation coefficients between significantly responsive PV and PC neurons of one imaged region. Cells were ordered such that the strongest correlations during spontaneous activity were close to the diagonal in the spontaneous condition, and the same order was applied to correlation matrices of the other conditions. Positions on the diagonal were set to the lowest value. **h.** The similarity between two matrices is the correlation coefficient of their off-diagonal elements (pattern correlation). Comparisons were made between correlation matrices of spontaneous and each of the evoked conditions, and between different visually evoked conditions for PC cells (green), PV cells (red) and for matrices from mixed PC/PV pairs (black). Boxplots represent median values of all imaged regions that included three or more responsive PV cells (vertical lines are group medians, 6 animals, 13 regions).

Europe PMC Funders Author Manuscripts

Europe PMC Funders Author Manuscripts

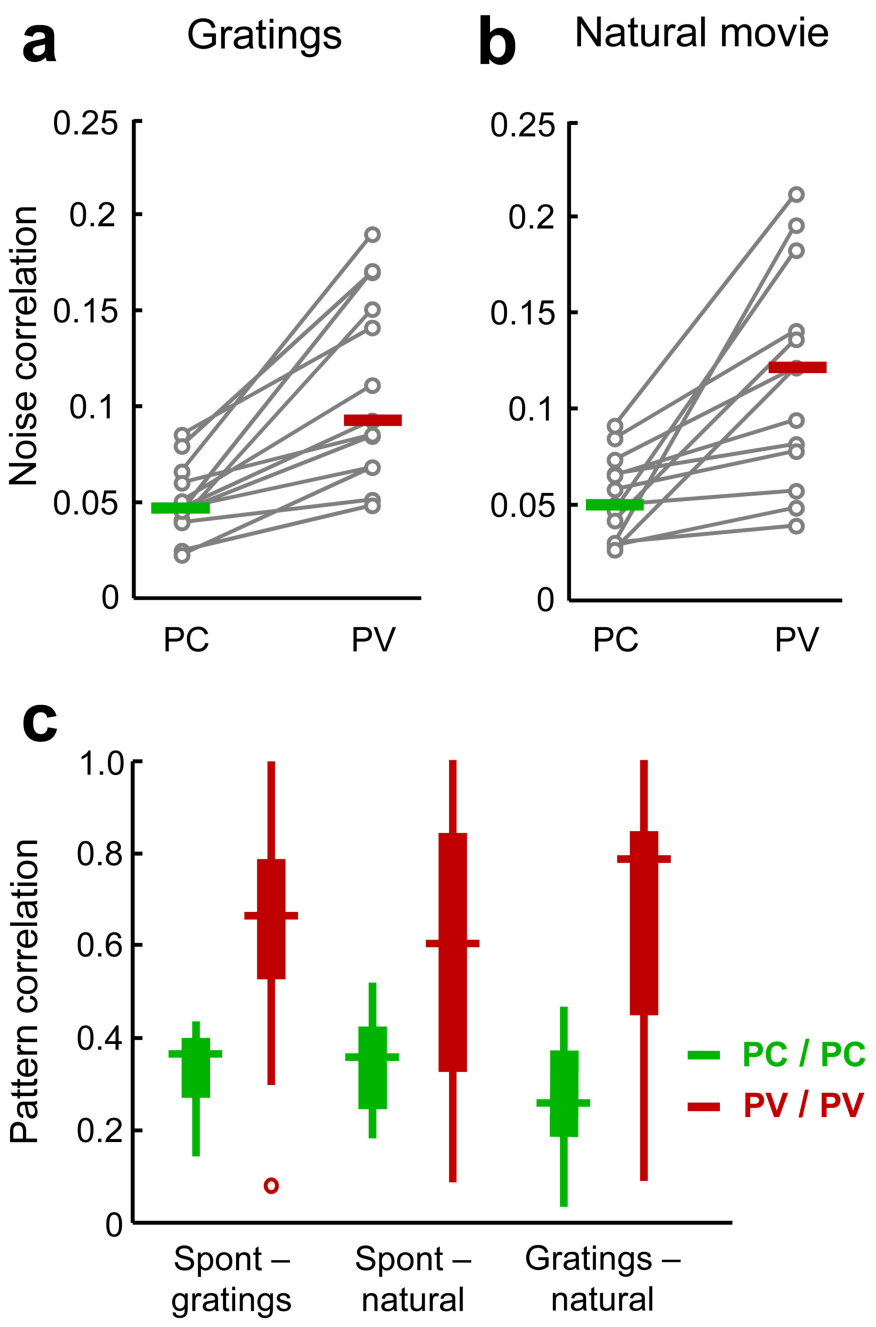

Figure 5. Comparison of spontaneous and noise correlation patterns during visual stimulation.

a,b. Noise correlation coefficients from calcium signals during stimulation with drifting gratings (**a**) or with natural movie sequences (**b**) for PC cell pairs (left, green) and PV cell pairs (right, red). Circles depict median values of each imaged region, colored lines indicate group median. **c.** Similarity of matrices of noise correlations during visually-evoked conditions (see Methods) and correlations during spontaneous activity (left and middle) and similarity of noise correlation matrices during grating and natural movie stimulation (right) for PC (green) and PV (red) cell populations. Pattern correlation values are correlation

coefficients of off-diagonal matrix elements for each imaged regions with three or more responsive PV cells, 6 animals, 13 regions.

Europe PMC Funders Author Manuscripts